



HAL
open science

Design and performance of an E-band chirped pulse spectrometer for kinetics applications OCS – He pressure broadening

Brian M. Hays, Théo Guillaume, Thomas Hearne, Ilsa R. Cooke, Divita Gupta, Omar Abdelkader Khedaoui, Sébastien D. Le Picard, Ian R Sims

► To cite this version:

Brian M. Hays, Théo Guillaume, Thomas Hearne, Ilsa R. Cooke, Divita Gupta, et al.. Design and performance of an E-band chirped pulse spectrometer for kinetics applications OCS – He pressure broadening. *Journal of Quantitative Spectroscopy and Radiative Transfer*, 2020, 250, pp.107001. 10.1016/j.jqsrt.2020.107001 . hal-02638438

HAL Id: hal-02638438

<https://univ-rennes.hal.science/hal-02638438>

Submitted on 29 May 2020

HAL is a multi-disciplinary open access archive for the deposit and dissemination of scientific research documents, whether they are published or not. The documents may come from teaching and research institutions in France or abroad, or from public or private research centers.

L'archive ouverte pluridisciplinaire **HAL**, est destinée au dépôt et à la diffusion de documents scientifiques de niveau recherche, publiés ou non, émanant des établissements d'enseignement et de recherche français ou étrangers, des laboratoires publics ou privés.

Design and performance of an E-band chirped pulse spectrometer for kinetics applications: OCS – He pressure broadening

Brian M. Hays, Théo Guillaume, Thomas S. Hearne, Ilsa R. Cooke, Divita Gupta, Omar Abdelkader Khedaoui, Sébastien D. Le Picard, and Ian R. Sims*

Univ Rennes, CNRS, IPR (Institut de Physique de Rennes) - UMR 6251, F-35000 Rennes, France

*Author to whom correspondence should be addressed. email : ian.sims@univ-rennes1.fr

Abstract

Product channel-specific reaction kinetics at low temperature presents a significant challenge for both experiment and theory but provides essential inputs for astrochemical models of cold interstellar environments. Reaction kinetics studies using chirped pulse Fourier transform microwave (CP-FTMW) spectroscopy provide a potential solution but require the use of a buffer gas to thermalize the reactants and products; however, collisions with the buffer gas reduce the length of the detected signal, the free induction decay, through pressure broadening. The effect of this on time domain signals is largely unexplored using CP-FTMW spectrometers. A new E-band (60-90 GHz) spectrometer has been constructed using previously unavailable equipment in order to maximize its performance for detecting molecules in collisional environments. The design of this spectrometer is described in detail. The pressure broadening of OCS in He was used to test the spectrometer under collisional conditions similar to those that are routinely used to perform reaction kinetics measurements. The corresponding pressure broadening coefficients for transitions in this frequency range were determined at room temperature and the performance of the spectrometer was assessed in relation to recently reported chirped pulse in uniform flow experiments.

Keywords Chirped Pulse Fourier Transform Spectroscopy, Free Induction Decay, Millimeter Wave Spectroscopy, Pressure Broadening, Carbonyl Sulfide

This project has received funding from the European Research Council (ERC) under the European Union's Horizon 2020 research and innovation programme (grant agreement No 695724-CRESUCHIRP).



1. Introduction

The formation of molecules in interstellar space can be described using astrochemical models, which are supplied information from many sources including chemical kinetics [1]. Experimental studies of gas-phase bimolecular reaction kinetics at temperatures relevant to the cold interstellar medium (10–100 K) was difficult until the invention of the CRESU (Cinétique de Réaction en Ecoulement Supersonique Uniforme, or reaction kinetics in uniform supersonic flow) technique [2,3]. The CRESU technique creates a relatively dense environment (10^{16} – 10^{17} cm⁻³), at supersaturated conditions, which thermalizes reagents and products to low temperatures via collisions within a cold buffer gas flow. To investigate chemical kinetics with the CRESU technique, laser spectroscopy has most often been used to detect species of interest with high sensitivity, but this spectroscopic technique can only follow one reactant or product at a time [3]. Multiplexed detection of products by tunable VUV synchrotron photoionization mass spectrometry has been applied with great success to the determination of product branching ratios at room temperature and above [4–6], and using a pulsed version of the CRESU technique to a few reactions down to 70 K [7,8].

Recently, the Chirped Pulse in Uniform Flow (CPUF) technique has been developed to address the problem of product branching ratios [9,10]. It combines the CRESU technique with Chirped Pulse Fourier Transform Microwave spectroscopy (CP-FTMW) [11]. Using this technique, branching ratios of astro-chemically relevant reactions could be measured experimentally at temperatures as low as 22 K [12]. However, the signal used to monitor CP-FTMW experiments, the Free Induction Decay (FID), is significantly quenched in the relatively high-pressure environment of a typical CRESU experiment. This quenching of the FID in the time-domain is directly related to pressure broadening in the frequency domain. But for time domain experiments, pressure broadening has a sinister effect: reduction of signal-to-noise ratio by reducing the duration of the detectable signal.

Microwave spectroscopy has typically been performed in the cold, collision-free environment of a molecular beam or free jet expansion, which is ideal for spectroscopic studies [11,13]. These environments are unsuitable for directly studying bimolecular reactions and dynamics, where collisions are essential. Gas-phase bimolecular reaction kinetics is usually studied in the presence of a buffer gas so that excess energy from reactant preparation or product formation can be thermally equilibrated. Some studies using CP-FTMW spectrometers have been performed in environments where collisions are relevant [14–18], but the effect of collisions on these spectra has received little attention using new

instrumental techniques. Given the importance of collisional environments to the study of reaction kinetics, the effect of collisions on CP-FTMW spectra is of great interest.

Pressure broadening is a well-known phenomenon where spectral transitions are broadened to a width proportional to the pressure in the environment. In time-domain experiments, pressure broadening contributes to the speed of the decay of the FID, known as the dephasing rate. The effects of pressure dephasing have been examined in cold buffer gas cells using a CP-FTMW spectrometer, where pressure broadening coefficients of transitions from a few molecules were measured at very low temperatures, and very large pressure broadening coefficients were found [14]. Using a CP-FTmmW (where mmW stands for millimeter wave and replaces MW in the former acronym) spectrometer, the Doppler effect was directly fit to a single transition FID to measure the mass of different molecular species after the pressure component of a Voigt profile was found using Hahn echo experiments [15,16]. Recently, self-broadening pressure coefficients of OCS and ammonia were fit at room temperature [17,18], but without a buffer gas, reducing the relevance of these experiments to the CPUF technique. To simulate these conditions, OCS pressure broadening in excess He has been investigated in the present study up to pressures comparable to CRESU experiments.

OCS is a favorable molecule for microwave and millimeter wave experiments as it has quite intense transitions, and He will be the buffer gas used in future CPUF experiments. The pressure broadening coefficients for the OCS + He system have been studied for many years, usually using microwave spectroscopy [19–24] but also with infrared spectroscopy [25]. Theoretical pressure broadening cross-sections have been calculated using a semiclassical relaxation theory [26] and the infinite order sudden approximation from a potential energy surface of OCS + He [27], the latter of which was compared against experimental data and found to disagree quite dramatically [21,25]. A new potential energy surface was calculated for investigating the He-OCS van der Waals complex [28], which was then used to obtain state-to-state rotational energy transfer rate coefficients below 150 K for the collisional system [29]. The potential was then used for calculating low-temperature pressure broadening cross sections for direct comparison to experimental values. The theoretically calculated pressure broadening cross sections matched experimental transitions fairly well at 20 K, but discrepancies between theory and experiment became larger at lower temperatures [22]. The compilation of OCS + He pressure broadening data in the HITRAN database points to the scarcity of data in general for this collisional system [30].

As more experiments using CP-FTMW spectroscopy move towards observing molecules in collisional environments, collisional effects on FIDs should be examined in detail. In the context of the CPUF

technique, this needs to be related to conditions where molecules will be examined for kinetics purposes in collisional environments using CP-FTMW spectroscopy. We briefly review the dephasing model used in this study, before describing a new CP-FTMW spectrometer that has been built in the millimeter wave region to determine the product channel branching ratios of chemical reactions. The details and its basic performance characteristics are discussed. The effects of pressure on the FIDs are examined using the OCS + He system, and the data fit using a time domain Voigt profile. The results are compared to previous data on the OCS + He system, also extending the data on this system to previously unstudied transitions. Furthermore, the effect of the high-pressure conditions on the molecular FID is discussed as it pertains to signal analysis, signal-to-noise ratio, and the performance of this spectrometer under conditions relevant to the examination of reaction kinetics.

2. Dephasing Model

The signal recorded in a CP-FTMW spectrometer is the FID, which is the characteristic decay back to equilibrium of a sample polarized by an external electric field. This polarization is described by the optical Bloch equations [31]. For the linear fast passage regime in which most microwave or millimeter wave chirped pulse spectrometers aim to operate, the polarization magnitude has been solved before for chirps [32–35], as well as for situations using only $\pi/2$ single frequency pulses [35,36], which most CP-FTMW spectrometers are capable of producing. We focus here on the shape of the FID after the polarizing pulse is turned off and the dipoles are freely precessing.

The simplest description of the shape of the FID is given only in terms of homogeneous decay, dictated by the phenomenological decay constant T_2 in the optical Bloch equations [35]. This describes the decay of coherence within a polarized system, which includes the rate of decay by collisional rotational inelastic energy transfer, as well as elastic or phase changing collisions [37]. The decay constant T_2 is related to the pressure broadening rate by $T_2 = 1/(2\pi\gamma_{pres}p)$, where γ_{pres} is the pressure broadening coefficient. The linewidth of a pressure broadened signal in the frequency domain is thereby related to the decay time of the polarized sample in the time domain. Microwave spectroscopy is frequently performed in the limit where Doppler broadening or decay is the dominant dephasing mechanism. The shape of the FID is no longer dominated by the pressure decay rate and must include the Doppler decay rate. Within this limit, a simple form of the exponential decay function fails to describe the system and it is necessary to include a Gaussian type function as well [38].

Experiments to monitor pressure broadening in FIDs were among the first performed using FTMW techniques. The first experiments often measured self-broadening rates, using OCS [39] and NH₃ [40], where pressure broadening decay rates are high enough that the Doppler decay could be ignored. Collisions with foreign colliders, at first, did not include Doppler broadening in their fitting of experimental data [19]. Later, Mäder and coworkers studied pressure broadening rates between different molecules and various rare and diatomic gas colliders, where accurately accounting for Doppler decay was important for disentangling the pressure decay rates [41–46] specifically using the time domain Voigt profile. The decay profile was used for both line position and pressure broadening determination, as it yielded quite accurate results for both [47]. Eventually, this profile was superseded with the inclusion of the speed dependence of collisions [48,49], but this additional rate of relaxation was found to have minimal effect on He collisions with other molecules [50].

The time domain Voigt profile is the Fourier transform of the commonly used Voigt function, which is a convolution of the Gaussian and Lorentzian functions, representing the Doppler and pressure broadened components of a transition profile. Equation 1 shows the time domain Voigt profile taken from the derivation of the Fourier transform of a Voigt function for use in spectroscopy [51]:

$$f(t) = A \exp\left(-2\pi\Delta\nu_{Pres}t - \frac{\pi^2\Delta\nu_{Dopp}^2 t^2}{\ln(2)}\right) \cos(2\pi\nu_0 t + \theta) \quad \text{Eqn. 1}$$

where $f(t)$ is the signal intensity as a function of time, A is the initial amplitude of the FID, $\Delta\nu_{Pres}$ is the pressure broadening rate, $\Delta\nu_{Dopp}$ is the Doppler broadening rate, ν_0 is the center frequency of the transition, and θ is the phase of the signal. The phase and amplitude fitting parameters were included in Eqn. 1 from comparison with the equation used by Haekel and Mäder, where these parameters were found to have assisted in the fitting of experimental data [47].

The measured pressure broadening rate $\Delta\nu_{Pres}$ is related to the temperature dependent pressure broadening coefficient $\gamma_{Pres}(T)$ by $\Delta\nu_{Pres} = \gamma_{Pres}(T) \times p$, where p is pressure. By plotting $\Delta\nu_{Pres}$ vs. p , the pressure broadening coefficient can be found at a specific temperature. The Doppler decay rate is the Doppler half width at half max (HWHM) of the frequency domain signal. The fitting model used by Haekel and Mäder constrained the Doppler component to its theoretical value [47], but in this study it was found that the Doppler component could be fit along with the other fitting parameters in the model at low pressures and high signal-to-noise using a non-linear least squares fitting algorithm [52].

3. Experimental

A new chirped pulse Fourier transform millimeter wave (CP-FTmmW) spectrometer operating in the E-band has been constructed, incorporating numerous advances in millimeter wave technology that had not been available to previous spectrometers operating in this frequency range [12,34,53,54], but were available to spectrometers operating at lower frequencies [11]. In particular, a PIN diode switch and a low noise amplifier (LNA) operating at E-band frequencies were purchased from commercial vendors. Furthermore, relatively high-power amplifiers for this frequency range were used to maximize the polarizing signal. A schematic of the spectrometer is shown in Fig. 1.

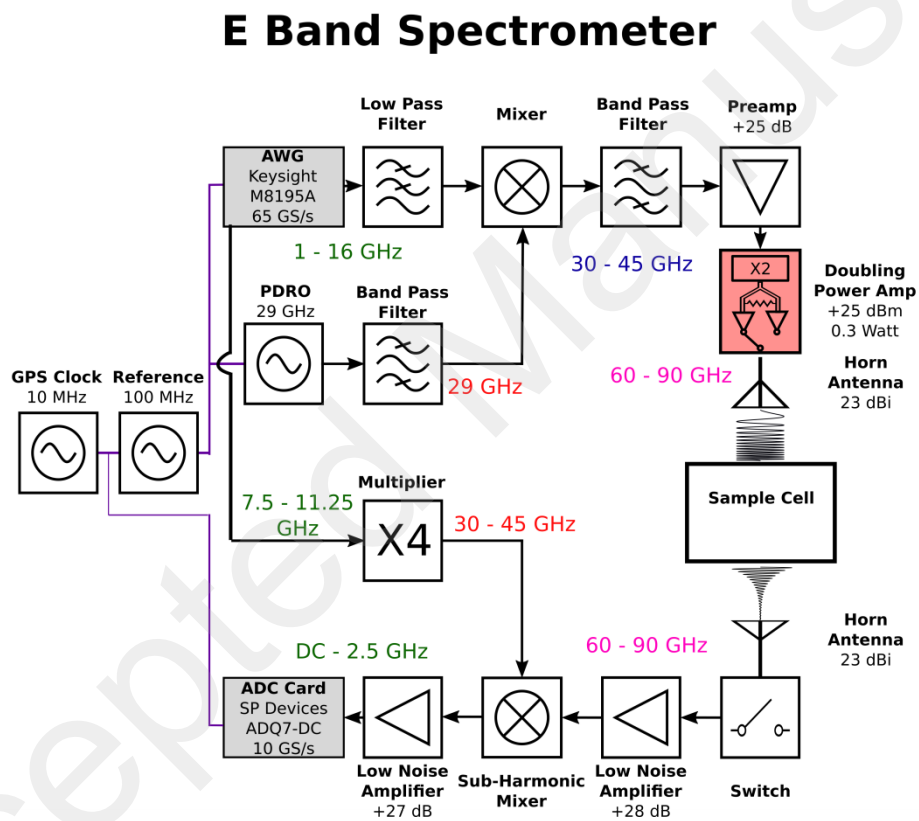


Fig. 1: Schematic of the E-band spectrometer.

The up-conversion side of the spectrometer is similar to the design of Zaleski et al., but accomplished at a higher frequency range [55]. An arbitrary waveform generator (AWG, Keysight M8195A, 64 GSa/s) was used to produce frequencies in the range of 1-16 GHz. The signal from the AWG was up-converted in a mixer (Marki M11850H) using a phase-locked dielectric resonator oscillator (PDRO, Microwave Dynamics PLO-2070-29.00) operating at 29 GHz as the local oscillator (LO) source. The upper sideband is selected using a broadband high-pass filter (Reactel 9HS-X30/45G-K11R) before entering the preamplifier (Quinstar

QPW-205020525-J0). This signal is then input into a Quinstar integrated system (QBM-609025E0U0R) that includes a passive frequency doubler to bring the frequency range to 60-90 GHz (Quinstar QPM-75002E), a waveguide splitter (Quinstar QJH-EUFBZIL), two millimeter wave power amplifiers (Quinstar QPW-60752530-C2W0 and Quinstar QPW-75902530-C2W0), and a waveguide switch (Quinstar QWZ-ET2800). One amplifier operates between 60-75 GHz while the other operates between 75-90 GHz. Both amplifiers output about 300 mW of RF power over each band, with significant power up to 94 GHz for the higher frequency amplifier. The amplifiers are controlled via TTL signals for fast turn-on and turn-off times of less than 20 ns. The waveguide switch is a low-loss (0.7 dB) but slow (50 ms) electro-mechanical switch which selects the amplifier to be used. The radiation is output through a 23 dBi gain horn antenna (Quinstar QWH-EPRR00).

The receiver system incorporates many advances in commercial millimeter wave technology, especially high frequency LNAs and switches that were mentioned but unavailable when Park et al. made their first high frequency spectrometer in 2011 [34]. The start of the receiver system is an identical horn antenna (Quinstar QWH-EPRR00) followed by a variable attenuator that attenuates signals by up to 30 dB (Quinstar QAL-E00000), for monitoring pulse power while running experiments. The signal then enters a fast single pole-single throw PIN switch operating in the 60-90 GHz range (Millimeter Wave Products 911E/387TTL). The switch has a 10 ns 10%-90% rise time to either transmission or isolation, with around 3 dB insertion loss across the band, and over 30 dB of isolation. This switch protects the next element, the millimeter wave LNA, from the initial polarizing pulse. The LNA (Millitech LNA-12-02350) has (28 ± 4) dB of gain across the 60-90 GHz range. It has a 3 dB noise figure, rising to 4.5 dB below 67 GHz. After the low-noise amplifier is a subharmonic mixer (Virginia Diodes WR12SHM), which has a dual sideband conversion loss of 6 dB with a 3 dB bandwidth of DC-15 GHz at the intermediate frequency (IF) port. The output from the IF is further amplified using a LNA with 25 dB of gain and a 2.5 dB noise figure (Miteq AFS4-00101800-25-S-4). The choice of the LO source is determined by whether an oscilloscope or a digitizer card is used to record the heterodyned signal. The LO can come from one of two sources: a PDRO operating at 37.5 GHz (Microwave Dynamics PLO-2070-37.50) or the second channel of the AWG sent through a quadrupler (Quinstar QMM-38150504J) providing an LO between 30-45 GHz.

The oscilloscope is a Tektronix DPO 71604C with 16 GHz of analog bandwidth and is capable of running at 100 GSa/s; however, it is normally used at 50 GSa/s for faster data processing. The oscilloscope provides broadband capabilities as well as flexible modes of operation, particularly FastFrame (a proprietary software from Tektronix). However, the oscilloscope cannot operate multiplexed acquisition schemes at

the processing speeds needed for high data throughput experiments, so a digitizer is used when high speed acquisition is needed. The digitizer is a Teledyne SP Devices ADQ7DC-PCIE card running at 10 GSa/s with a 2.5 GHz 3 dB bandwidth.

The oscilloscope and digitizer were triggered by pulses from an AWG marker channel. The switch and pulsed amplifiers were controlled by a BNC 575 digital pulse/delay generator (DDG), which was triggered by another marker channel on the AWG. Each cycle of the experiment was conducted in a manner to protect the low noise receiver from the intense polarizing pulse, so that the polarizing pulse does not damage the LNA. Most of the system, particularly the AWG, the PDRO's, and the oscilloscope, was synchronized to a 100 MHz oven-controlled crystal oscillator (Precision Test Systems GPS10-eR-50) which was locked to a GPS-disciplined Rb clock (Stanford Research Systems FS740) operating at 10 MHz. The higher-frequency 100 MHz signal was used to improve phase stability compared to the lower-frequency 10 MHz standard [53]. The digitizer and the DDG were synchronized to the 10 MHz clock.

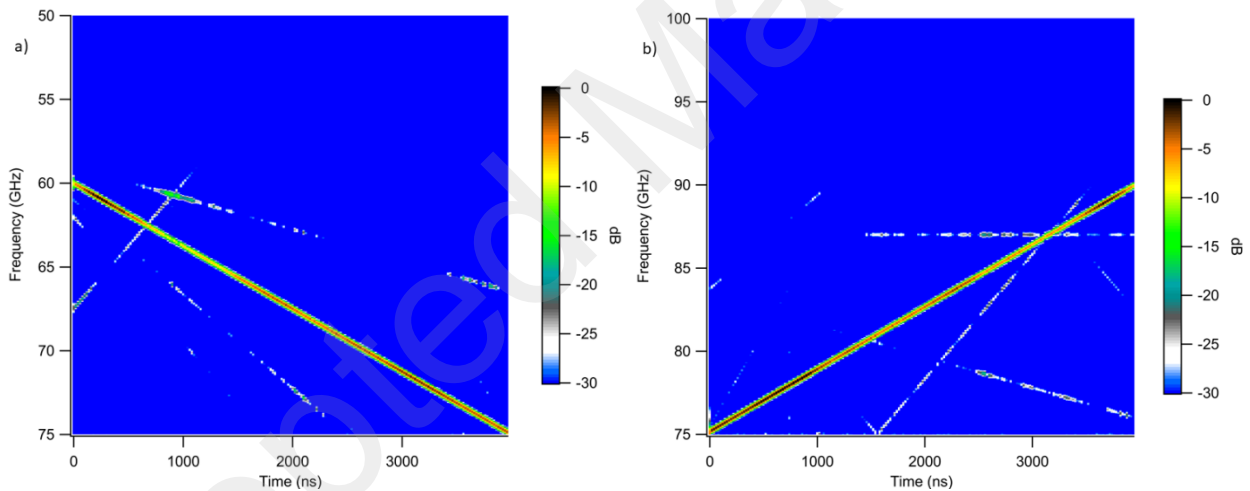


Fig. 2: Spectrograms of a) 60—75 GHz (15 GHz—DC at IF) and b) 75—90 (DC—15 GHz at IF) are shown. The dynamic range is 30 dB. The spectrograms in plot a) are 2 dB higher in total intensity.

The spectral purity of a chirp across each band was measured using the oscilloscope with the PDRO as a LO source and without the LNAs or the switch in the signal path. An attenuator was used before the mixer to ensure that the high-powered chirped pulse signal would not exceed the linear response regime. The PDRO provides a pure and filtered LO source for down-conversion, while the oscilloscope provides a wide bandwidth of 16 GHz with flat frequency response of ± 0.5 dB using digital signal processing within the oscilloscope. Frequency chirps lasting 5 μ s, extending across the full bandwidth of each amplifier, were used to test the frequency response of the transceiver. Spectrograms were constructed using 1000 time

points per spectrum with 198 spectra, and are shown in Figure 2a (60—75 GHz) and Figure 2b (75—90 GHz). The spectral response of the system was found to vary by about 5 dB across the bandwidth with major spurs recorded at less than 20 dBc, as can be seen in Figs. 2a and 2b. The major exception to this is around 64 GHz, where there was a significant reduction in the intensity of the main signal as well as an increase in the spurious content. This spur can be reduced by providing more power directly into the doubler, but this compresses the signal at other frequencies and introduces unwanted, sharp intensity variations. The up-conversion scheme produces some harmonic spurs, but these were not the dominant spurs in the spectrum. However, a third harmonic of the up-conversion PDRO did bleed through into the chirp in the higher frequency band. Higher input power into the integrated system increases harmonic content without increasing the overall spectral intensity, indicating that the overall system was operating near compression or saturation.

The switches currently available in the E-band are not as high performance as those in lower frequency spectrometers; the isolation is often below 40 dB. However, with short chirps the electronics do not seem to have reached damage threshold, especially in the high frequency LNA and sub harmonic mixer. There is, however, some recovery time observed that appears to be purely electronic due to the high power of the polarizing pulse bleeding through the switch.

When using the digitizer, the PDRO was replaced with the quadrupled output of the AWG as the LO. Using the same reference source as the pulse production in the receiver helps reduce phase fluctuations [56]. This provided a LO source that allowed the digitizer to cover the entire range of the spectrometer in segments [57]. The digitizer is capable of fast averaging, recording up to 200 μ s of 14 bit data at 10 GSa/s up to 262144 times in an FPGA accumulator with a 20 ns rearm time. High duty cycle experiments can be performed in this mode of operation, as well as experiments using a wide variety of pulse sequences over the recording time. The digitizer can complete a 200 μ s collection cycle 10^5 times in less than a minute, running at a rate higher than 4.5 kHz with a duty cycle higher than 90 %. However, these experiments were performed at about 20 % duty cycle.

The combination of the digitizer with the quadrupled AWG output as the LO introduced some issues. The quadrupler is not as pure a source for the LO as the PDRO and introduced spurious content into the spectrum. The digitizer also introduces strong spurs, particularly at 5 GHz, 2.5 GHz, 100 MHz, and 10 MHz, into the spectrum. These mostly come from clock inputs whereas the 5 GHz spur likely occurs from the slight DC offset produced from the interleaving of the two analog to digital converters (ADCs) within the digitizer. The 5 GHz spur was easily filtered during post processing. However, the interaction between the

LO source, the mixer, and the digitizer appears to have produced several spurious frequencies that were always present in recorded spectra. These may have been due to spurious LO signals mixing together within the mixer [16]. The spurious signals were cancelled out in the time domain using a correlation filter, similar to the way the mismatched ADCs were removed from spectra taken with another digitizer [58]. This is effective for removing electronic spurs but not for intermodulation spurs [55]. Each record lasts well past when the FIDs are no longer detectable, providing extra points at the end of the time domain acquisition to use in a background subtraction. Multiples of 800 points were averaged together and subtracted from the whole time domain trace, resulting in the unwanted coherent spurs at particular frequencies being subtracted out but not the noise or molecular emission. Care must be taken to ensure that the molecular emission is not included in the samples taken for the background subtraction; therefore 100 multiples of 800 points were taken, accounting for 8 μ s at the end of the recorded sample, which was after the FID signal was below the noise level even at low pressures for these experiments.

Spectra were obtained using a 16 cm diameter 1.5 m long flow cell. The walls of the flow cell were lined with millimeter wave absorptive foam (Eccosorb HR-10 Laird) to reduce reflections while recording the FID. The unfocused radiation was output from the waveguide horn through a wedged Teflon window into the flow cell, and at the end of the flow cell the radiation exiting through another Teflon window was collected with another waveguide horn into the receiver. A 1% OCS in He mixture was flowed into the cell through a mass flow controller (Brooks GF080CXXC) at a constant flow rate, while another flow controller passed pure He into the flow cell. Only the pure He flow controller was adjusted to change the pressure in the flow cell, keeping the partial pressure of OCS constant throughout each experiment. OCS was purchased from Sigma Aldrich (97.5% purity) and the He was from Air Liquide (99.995% purity). Two different pumping setups were used to evacuate the flow cell: one used a turbomolecular pump for low pressure experiments below 0.03 mbar and the other used a throttled roots blower system for the high pressure experiments, up to 0.35 mbar. The pressures in the flow cell were measured using capacitance manometers (Brooks XacTorr CMX0). The partial pressure of OCS was around 2×10^{-5} mbar when using the turbomolecular pump and 5×10^{-5} mbar when using the roots blower system.

Three pure rotational transitions of OCS within the range of the E-band were examined: $J=5-4$, $J=6-5$, and $J=7-6$. These transitions were pumped using resonant single frequency pulses that were 1 μ s long, with the FID being recorded up to 20 μ s. 10^5 averages were taken in less than 1 minute for each transition using the digitizer setup. Filtering techniques described above were used while further analysis was performed using bespoke Igor Pro routines.

4. Results

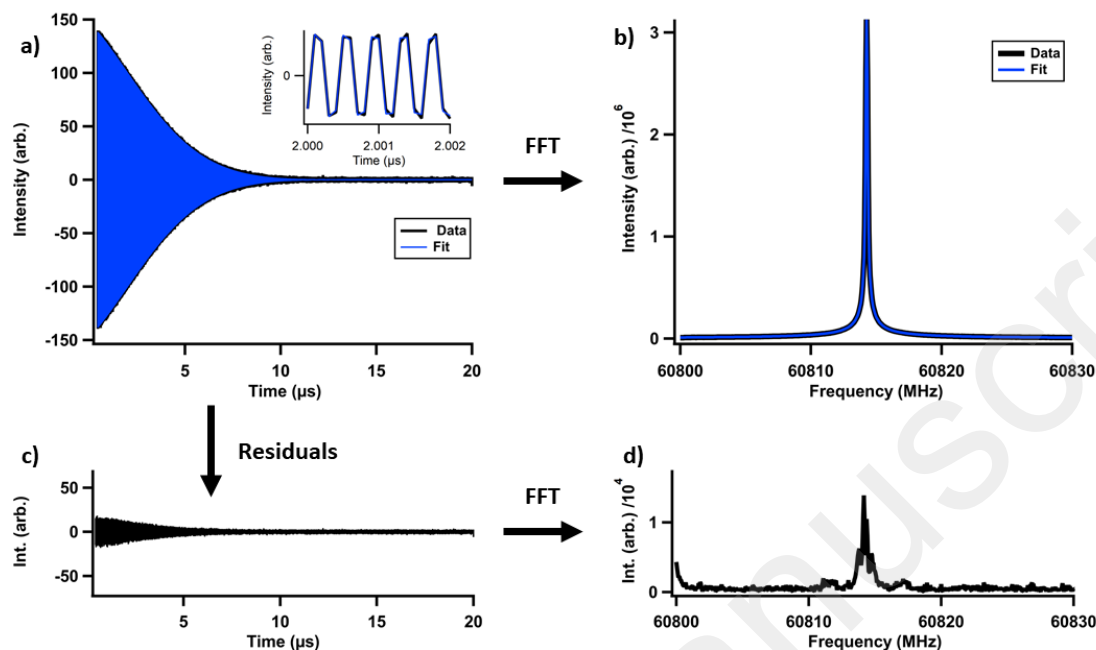


Fig. 3: The $J=5-4$ transition of $\sim 5 \times 10^{-5}$ mbar OCS in 5×10^{-3} mbar of He. a) The FID (black) fit to the time domain Voigt model (blue). An inset shows the quality of the fit over 2 ns. b) The Fourier transform of the data (black) and the fit (blue). c) The residuals between the data and the fit in the time domain, with the same (arbitrary) intensity units as in a), spurs being the largest decaying signal. d) The Fourier transform of the time domain residuals around the transition frequency, with the same (arbitrary) intensity units as in b) but displayed at 200 times magnified scale.

We examined three transitions of OCS broadened by He using the newly described spectrometer. Figs. 3 and 4 show a low pressure FID and a high pressure FID respectively along with their fast Fourier transforms (FFT), as well as the residuals resulting from the subtraction of the data from a fit to the time domain Voigt model (eq. 1), all for the $J=5-4$ transition. The high degree of averaging allowed for extremely high signal-to-noise in the low-pressure regime, in both time and frequency domain data, as shown in Figures 3a and 3b. A rectangular window was applied to the time domain signal before the FFT in order to retain the decay characteristics in the line profile in the frequency domain, which differs from many other chirped pulse experiments where different windowing functions were applied [11]. A 20 μs long window was used with the FFT on the low-pressure data to maximize frequency accuracy, resulting in a full width at half maximum (FWHM) of ~ 0.2 MHz for the measured OCS transition. The high-pressure data of OCS in He is shown in Figs. 4a and 4b. The signal-to-noise is significantly reduced compared to the low-pressure data, despite the same partial pressure of OCS being used. Only a 2 μs long window was used for the FFT of the high-pressure data due to this extremely fast dephasing. Extending the window of the FFT for pressure broadened FIDs was found to be unnecessary after twice the decay time [17]. The resulting transition had a FWHM of ~ 2.5 MHz, due to the extremely short FID.

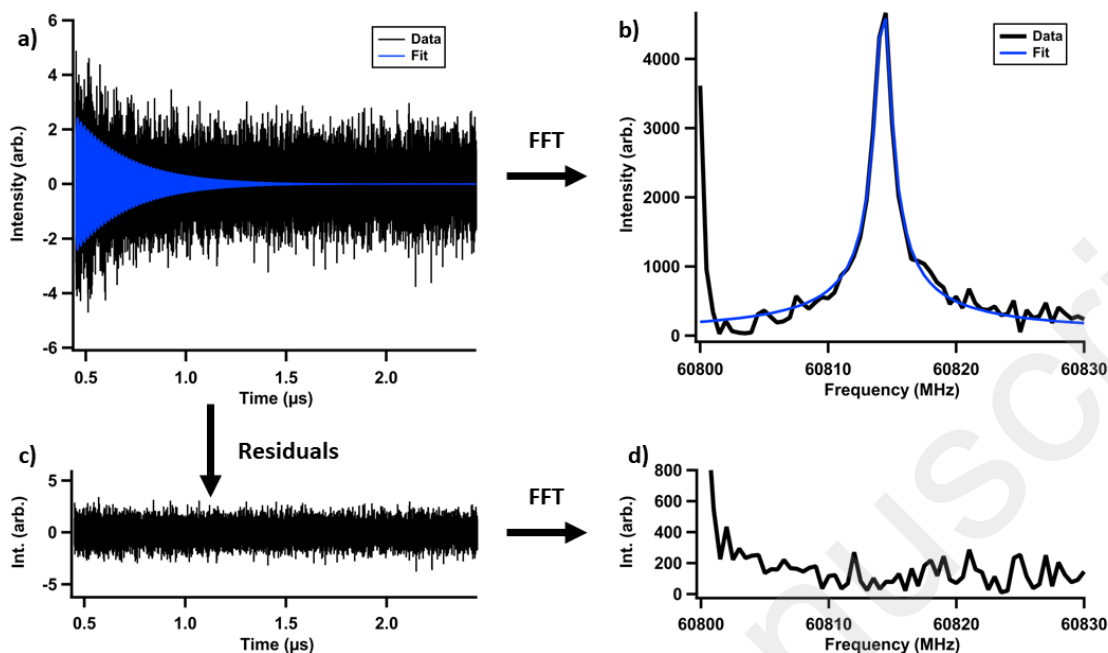


Fig. 4: The $J=5-4$ transition of $\sim 5 \times 10^{-5}$ mbar OCS in 0.239 mbar of He. a) The time domain FID (black) fit to the time domain Voigt model (blue). b) The Fourier transform of the data (black) and the fit (blue). c) The residuals between the data and the fit in the time domain, a) and c) have the same (arbitrary) intensity units. d) The Fourier transform of the time domain residuals around the transition frequency, with the same (arbitrary) intensity units as in b).

The FID for OCS in He was fit in the time domain using the time domain Voigt model (Eqn. 1). All of the parameters for the fitting model, in particular, the Doppler decay, were fit for the model shown in Fig. 3. At high pressures, the Doppler decay term was constrained while the other parameters were fit. The time domain Voigt model accurately reproduced the experimental signal, as shown in the Fourier transform of the residuals. The peak of the residuals is below 1% of the transition intensity, which indicates a high-quality fit of the experimental data.

The data taken at high pressures (Fig. 4a) was well fit by the model, producing a well-constrained pressure broadening coefficient for OCS and He even from low SNR data. The down-converted frequency placed the IF for this transition/LO combination close to the main clock spur of the digitizer at 2.5 GHz, present at the left of Fig. 4b. The correlation filter reduces the intensity of this spur, but cannot remove all of it even after high amounts of averaging. The time-domain fit only includes the desired transition without any effect from the close lying spur. While no residuals are above the noise level, there may be additional components to the FID that are below the noise level at this pressure which are not taken into account in the fit.

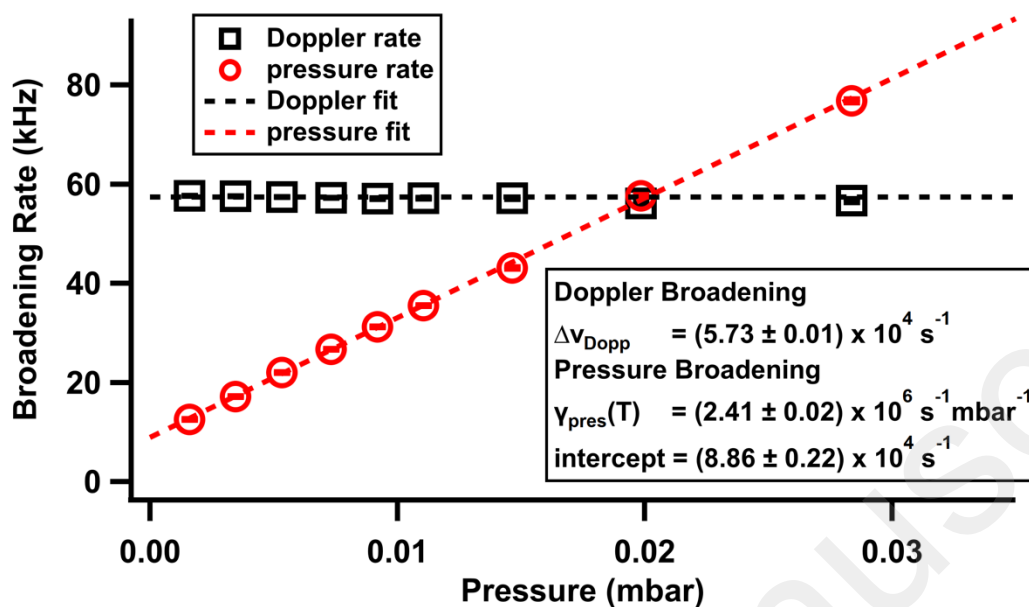


Fig. 5: Low pressure fits of Doppler and pressure broadening for the $J = 6 - 5$ transition of OCS ($\sim 2 \times 10^{-5}$ mbar) in He. The Doppler rate is constrained to zero slope, providing an average across the measured pressure range of (57.3 ± 0.01) kHz, while the pressure broadening rate is fit to a straight line whose slope yields the pressure broadening coefficient $\gamma_{pres}(T)$. Uncertainties are quoted at the 95% confidence interval.

Two experiments were performed to measure the pressure broadening coefficients of the OCS + He system using different pumping systems. First, a low pressure experiment was performed at pressures well below the crossover point between the Doppler and pressure broadening, so as to experimentally constrain Doppler broadening. The pressure and Doppler broadening rates obtained from the fits for the $J=6-5$ transition are shown in Fig. 5. The Doppler broadening fit was constrained to zero slope, effectively providing an average across the measured range of pressures. Error bars are represented on the graph but are typically a few orders of magnitude smaller than the magnitude of the constant that was fit, as the quality of the fits was quite high at low pressures. The Doppler rate was found to be within 1% of the expected value at 295 K for this OCS transition.

The results from higher pressure tests for the same transition are shown in Fig. 6, where exchanging the pumping group allowed the experiment to be performed at pressures up to 0.35 mbar. Noticeably, the pressure broadening rate was much faster at higher pressures than the Doppler broadening rate, so the Doppler rate Δv_{Dopp} was constrained in equation 1 to 57.3 kHz, the value obtained from the low pressure experiments. Fitting equation 1 at lower pressures produced well-constrained fitting parameters, while at higher pressures, especially above 0.25 mbar, the fit was found to be less robust due to the FID signal reducing towards the noise level in the time domain. At these high pressures, the decay has a time

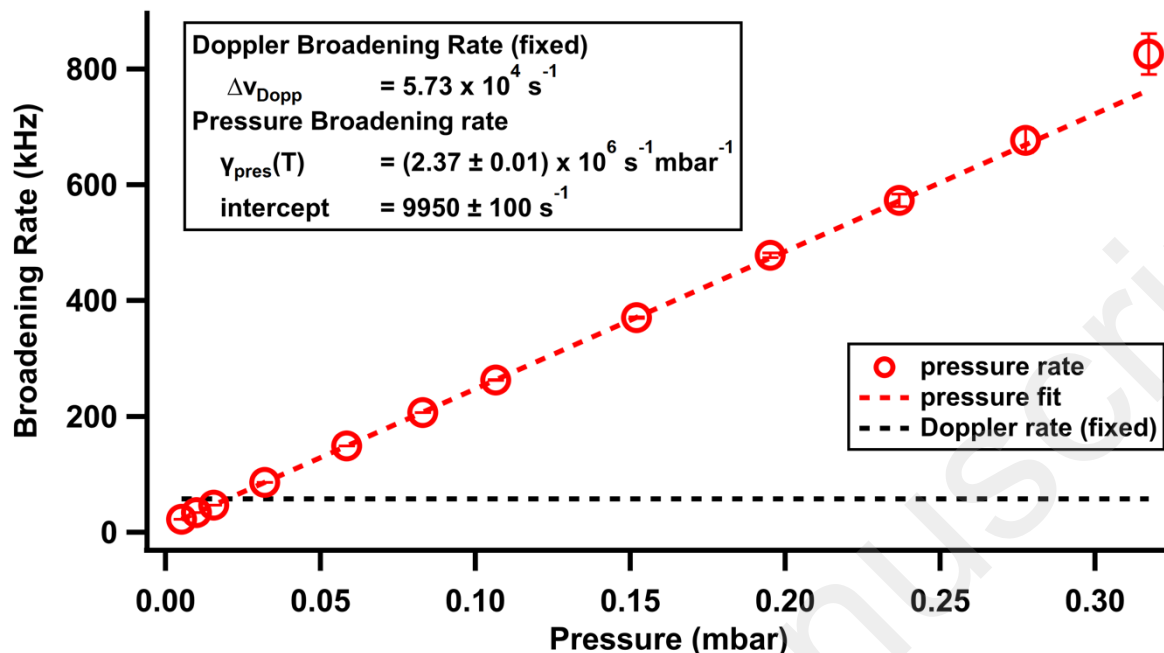


Fig. 6: High pressure fits of pressure broadening for the $J = 6 - 5$ transition of OCS ($\sim 5 \times 10^{-5}$ mbar) in He. The Doppler component was fixed to the value found in low pressure experiments. Uncertainties are quoted at the 95% confidence interval.

constant of around 200 ns, with very little data available for the fit. Except for pressures above 0.25 mbar, the pressure decay rates are well-represented by the linear fit. The pressure broadening coefficients of OCS in He at 295 K for each additional transition were found using the same analysis as shown in Figure 6 and described above, and all the measured coefficients are displayed in Table 1.

5. Discussion

The measured pressure broadening coefficients are compared against previously measured pressure broadening coefficients obtained using transient emission stark pulse spectroscopy [19], microwave spectroscopy [24], and infrared absorption spectroscopy [25] in Table 1. There is a transition with overlapping J levels between the infrared dataset and the current experiment, but from a P branch in an infrared band instead of a pure rotational transition, whose values should be similar. The difference between the previous experimental measurement of $J = 5-6$ and the measurement presented here for $J = 6-5$ is just beyond the combined uncertainties of both experiments. The value in the HITRAN database is a factor of two lower than those found here and in previous experiments [30].

Table 1: Measured OCS – He pressure broadening coefficients $\gamma_{Pres}(T)$ at 295 K with comparison to previous experiments and HITRAN. The uncertainties are quoted at the 95% confidence interval for the measurements reported here.

Transition	This experiment (MHz/mbar)	$\gamma_{Pres}(T)$	Previously published fits of $\gamma_{Pres}(T)$ (MHz/mbar)
HITRAN for unmeasured transitions			1.1 ^a
$J=1-0$			2.45 ± 0.04^b
$J=3-2$			2.5 ± 0.1^c
$J=5-6$ (P branch, ν_3)			2.6 ± 0.2^d
$J=11-10$ (R branch, ν_3)			2.2 ± 0.2^d
$J=5-4$	2.39 ± 0.01		
$J=6-5$	2.37 ± 0.01		
$J=7-6$	2.38 ± 0.01		

- a. Wilzewski JS, et al. [30]
- b. Mäder H, et al. [19] error 2σ
- c. Story IC, et al. [24] error rms
- d. Broquier M, et al. [25] error unknown

The theoretical data on the OCS + He collisional system are limited at room temperature. The theoretical pressure broadening cross sections used in Broquier et al. disagree dramatically from experimental values but agree qualitatively with the trend observed for different J levels of the OCS + He system. The theory predicted that the pressure broadening cross section should be higher at low J levels but reduce slightly with increasing J level before levelling off at higher J levels. The pressure broadening coefficients observed here are higher than those previously measured at high J levels but slightly lower than the previously observed $J=1-0$ transition, which indicates that the measured transitions are within the regime where pressure broadening depends upon J level. For a similar but more studied system, $\text{CO}_2 + \text{He}$, the trend of increasing pressure broadening coefficients with lower J was also observed [59]. The values reported here conform to the general trend predicted by theoretical pressure broadening cross section calculations.

The residuals presented in Fig. 3 indicate that the time domain Voigt profile (Eqn. 1) accounts for over 99% of the transition intensity. The remainder is expected to be small deviations in the profile caused by many possible effects, such as speed dependence of collisions [50], Dicke narrowing [60], or inhomogeneous fields [61]. This time domain Voigt profile has been shown in a previous study to fit almost all of the FID from CH_3F in He, but not with heavier buffer gases [50]. The high signal-to-noise achieved in the spectra presented here shows that even small deviations in line-shape can be observed in a relatively small short time, and further experiments could be used to investigate more advanced effects on line-shape profiles. A preliminary analysis of the data indicates that these techniques could be used to

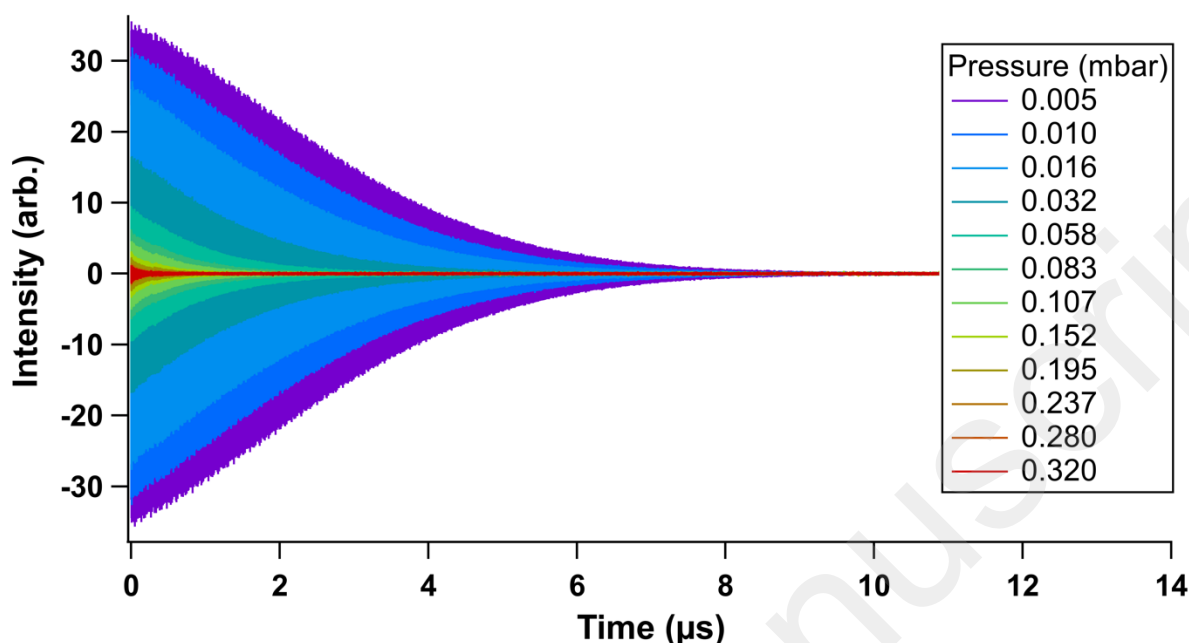


Fig. 7: Experimental FIDs for the $J=6-5$ transition over the experimental pressure range for a fixed partial pressure of OCS of 5×10^{-5} mbar in He buffer gas between 0.005 - 0.320 mbar.

determine line shift coefficients as well, but only within certain pressure ranges. No information on the line shift coefficients exist for the OCS + He system at room temperature, and so the initial results could not be compared against any previous work.

Fig. 7 shows FIDs from the $J=6-5$ transition recorded at different pressures. The effects of pressure broadening are seen in the change in the shape of the decays from Doppler dominated to pressure dominated with the exponential decay apparent at higher pressures. The initial signal amplitude can also be seen to be strongly attenuated as the He pressure was raised. The reduction in initial signal intensity was likely an effect of collisions on the polarization induced from the single frequency pulse, where the pulse time is longer than the T_2 time at higher pressures. As the pressure is raised in the experiment, the decay time becomes shorter than the pulse duration, with collisions disrupting the polarization of the sample. This effect is quite intense and means that at high pressures, even single frequency polarizing pulses can only effectively polarize for a limited amount of time. The reduction of initial signal is particularly strong at low pressures, where there is a sharp loss of initial signal amplitude before leveling out at high pressures.

The decrease in FID amplitude is much larger than expected over the pressure range, with multiple effects likely contributing to this. Due to experimental constraints, namely reflections within the system, the FID

was fit starting from 400 ns after the end of the excitation pulse. The FID decays rapidly during this time, reducing the available signal for fitting. As mentioned, the effective pulse length will shorten as T_2 starts to become the same magnitude or shorter than the pulse duration, reducing the polarization possible from a given pulse length. As the effective pulse becomes shorter, the frequency width of the pulse becomes greater, with less of the pulse overlapping with the frequency width of the transition. All of these effects will cause a reduction in initial FID amplitude, observed in these experiments, which makes excitation using single frequency pulses difficult to model. This difficult modelling can be avoided by using chirped excitation in the linear fast passage regime, which has a fast polarization time per transition, in order to describe the relative intensities of the signal. However, in this regime there are other effects, dependent on pressure broadening, that must be accounted for such as decay within the chirp and the importance of transition position within the chirp [9,17]. FID signals are inherently weaker in the linear fast passage regime compared to excitation via single frequency pulses, even when $\pi/2$ pulse conditions cannot be attained, so the types of pulses used here are still effective for experiments.

The new E-band spectrometer presented here has taken advantage of several recent technological advances in millimeter wave electronics that were unavailable to previous spectrometer designs but help to compensate for the reduced signal-to-noise ratios in pressure-broadened data. The power amplifiers used here can produce more powerful polarizing pulses than current active multiplier technology. To reduce the noise level of the receiver, the power amplifiers are pulsed to decrease the level of white noise from entering the receiver and a LNA has been added before the down-conversion mixer. The advantages of placing a LNA before a mixer in a receiver were recently discussed for emission spectrometers [62,63]. However, a blanking switch had to be employed to protect the LNA, which raised the noise temperature compared to the emission receivers. This is unavoidable when using high power amplifiers in the transmitter, to protect the high sensitivity electronics. Even with the blanking switch included, this design should result in a lower noise temperature in the receiver than designs that input directly into a mixer first before amplification. While the spectrometer performs very well when searching for weak signals, the optical path of the polarizing pulse presents a major issue. Reflections within the experiment persisted well into the record time, distorting the FID at early times. Reflections present a larger concern as the pressure rises. Since the FIDs become both shorter and weaker, the loss of signal can be significant compared to those obtained at low pressures. Removing reflections in the optical path would allow higher pressures and shorter FIDs to be recorded and analyzed with decent signal-to-noise ratio.

6. Conclusions

The OCS + He pressure broadening coefficients were determined using a new E-band CP-FTmmW spectrometer. The spectrometer was constructed to observe chemical reactions under conditions commonly used in kinetics studies, such as CRESU environments. Recently available components in millimeter wave technology were incorporated into the spectrometer, specifically to increase the sensitivity of this instrument when looking at signals in collisional environments. The performance of the spectrometer has been assessed using the OCS + He system, whose pressure broadening coefficients were measured up to pressures relevant to the CRESU technique. A time domain Voigt profile was employed to accurately represent the FID at both low and high pressures. The pressure broadening coefficients found here agree with previous work. The FID decays very rapidly at high pressures, which reduces the available signal for both time domain fitting and Fourier transformation. Furthermore, the initial amplitude of the FID is affected by the pressure, where the effective polarization of the polarizing pulse seems to be reduced as the pressure rises. These effects will compound in CPUF experiments, where the high pressures can reduce the detectable signal. Therefore, care must be taken to record as much of the FID as possible, especially at early times, to maximize the signal-to-noise ratio.

Experiments to examine reaction kinetics using CP-FTMW spectrometers usually require a buffer gas to thermalize the reactants and products of a reaction. The buffer gas causes dephasing of the probed transitions, leading to decay rates that correspond to pressure broadening coefficients in the frequency domain. Accounting for the rate of decay of a transition could be important when comparing relative intensities, as two transitions could have identical polarizations but differing rates of decay, which would lead to different intensities in the FT spectrum. Also, recording spectra under low pressure conditions with a buffer gas shows Doppler decay as a prominent feature of the FID, especially at room temperature. In higher pressure experiments, the time domain analysis presented here may prove to be beneficial to the analysis of spectra in pressure broadened samples.

Acknowledgments

The authors would like to thank Jonathan Courbe, Jonathan Thiévin, Didier Biet, Ewen Gallou, and Alexandre Dapp for technical support, and Kirill Prozument and Nadine Wehres for helpful discussions. The authors acknowledge funding from the European Union's Horizon 2020 research and innovation programme under the European Research Council (ERC) grant agreement 695724-CRESUCHIRP, and under

the Marie Skłodowska-Curie grant agreement 845165-MIRAGE. The authors are also grateful for support from the European Regional Development Fund, the Region of Brittany and Rennes Metropole. This work was supported by the French National Programme “Physique et Chimie du Milieu Interstellaire” (PCMI) of CNRS/INSU with INC/INP co-funded by CEA and CNES.

References

- [1] Wakelam V, Loison J-C, Herbst E, Pavone B, Bergeat A, Béroff K, et al. The 2014 KIDA network for interstellar chemistry. *Astrophys J Suppl Ser* 2015;217:20. <https://doi.org/10.1088/0067-0049/217/2/20>.
- [2] Dupeyrat G, Marquette JB, Rowe BR. Design and testing of axisymmetric nozzles for ion-molecule reaction studies between 20 °K and 160 °K. *Phys Fluids* 1985;28:1273–9. <https://doi.org/10.1063/1.865010>.
- [3] Cooke IR, Sims IR. Experimental Studies of Gas-Phase Reactivity in Relation to Complex Organic Molecules in Star-Forming Regions. *ACS Earth Space Chem* 2019;3:1109–34. <https://doi.org/10.1021/acsearthspacechem.9b00064>.
- [4] Osborn DL, Zou P, Johnsen H, Hayden CC, Taatjes CA, Knyazev VD, et al. The multiplexed chemical kinetic photoionization mass spectrometer: A new approach to isomer-resolved chemical kinetics. *Rev Sci Instrum* 2008;79:104103. <https://doi.org/10.1063/1.3000004>.
- [5] Lockyear JF, Fournier M, Sims IR, Guillemin J-C, Taatjes CA, Osborn DL, et al. Formation of fulvene in the reaction of C₂H with 1,3-butadiene. *Int J Mass Spectrom* 2015;378:232–45. <https://doi.org/10.1016/j.ijms.2014.08.025>.
- [6] Bourgalais J, Spencer M, Osborn DL, Goulay F, Le Picard SD. Reactions of Atomic Carbon with Butene Isomers: Implications for Molecular Growth in Carbon-Rich Environments. *J Phys Chem A* 2016;120:9138–50. <https://doi.org/10.1021/acs.jpca.6b09785>.
- [7] Soorkia S, Liu C-L, Savee JD, Ferrell SJ, Leone SR, Wilson KR. Airfoil sampling of a pulsed Laval beam with tunable vacuum ultraviolet synchrotron ionization quadrupole mass spectrometry: Application to low-temperature kinetics and product detection. *Rev Sci Instrum* 2011;82:124102. <https://doi.org/10.1063/1.3669537>.
- [8] Bouwman J, Fournier M, Sims IR, Leone SR, Wilson KR. Reaction Rate and Isomer-Specific Product Branching Ratios of C₂H + C₄H₈: 1-Butene, cis-2-Butene, trans-2-Butene, and Isobutene at 79 K. *J Phys Chem A* 2013;117:5093–105. <https://doi.org/10.1021/jp403637t>.
- [9] Oldham JM, Abeysekera C, Joalland B, Zack LN, Prozument K, Sims IR, et al. A chirped-pulse Fourier-transform microwave/pulsed uniform flow spectrometer. I. The low-temperature flow system. *J Chem Phys* 2014;141:154202. <https://doi.org/10.1063/1.4897979>.
- [10] Abeysekera C, Zack LN, Park GB, Joalland B, Oldham JM, Prozument K, et al. A chirped-pulse Fourier-transform microwave/pulsed uniform flow spectrometer. II. Performance and applications for reaction dynamics. *J Chem Phys* 2014;141:214203. <https://doi.org/10.1063/1.4903253>.
- [11] Brown GG, Dian BC, Douglass KO, Geyer SM, Shipman ST, Pate BH. A broadband Fourier transform microwave spectrometer based on chirped pulse excitation. *Rev Sci Instrum* 2008;79:053103. <https://doi.org/10.1063/1.2919120>.
- [12] Abeysekera C, Joalland B, Ariyasingha N, Zack LN, Sims IR, Field RW, et al. Product Branching in the Low Temperature Reaction of CN with Propyne by Chirped-Pulse Microwave Spectroscopy in a Uniform Supersonic Flow. *J Phys Chem Lett* 2015;6:1599–604. <https://doi.org/10.1021/acs.jpcllett.5b00519>.

- [13] Park GB, Field RW. Perspective: The first ten years of broadband chirped pulse Fourier transform microwave spectroscopy. *J Chem Phys* 2016;144:200901. <https://doi.org/10.1063/1.4952762>.
- [14] Patterson D, Doyle JM. Cooling molecules in a cell for FTMW spectroscopy. *Mol Phys* 2012;110:1757–66. <https://doi.org/10.1080/00268976.2012.679632>.
- [15] Harris BJ, Steber AL, Lehmann KK, Pate BH. *Gas Analysis by Fourier Transform mm-wave Spectroscopy*, Columbus, OH: 2013.
- [16] Harris B. *A Chirped Pulse Fourier Transform Millimeter Wave Spectrometer for Room Temperature, Gas Mixture Analysis*. University of Virginia, 2014. <https://doi.org/10.18130/v3vj8m>.
- [17] Hindle F, Bray C, Hickson K, Fontanari D, Mouelhi M, Cuisset A, et al. Chirped Pulse Spectrometer Operating at 200 GHz. *J Infrared Millim Terahertz Waves* 2018;39:105–19. <https://doi.org/10.1007/s10762-017-0445-3>.
- [18] Endres CP, Caselli P, Schlemmer S. State-to-State Rate Coefficients for NH₃–NH₃ Collisions from Pump–Probe Chirped Pulse Experiments. *J Phys Chem Lett* 2019;10:4836–41. <https://doi.org/10.1021/acs.jpcclett.9b01653>.
- [19] Mäder H, Ekkers J, Hoke W, Flygare WH. A π , τ , $\pi/2$ type pulse sequence method for the determination of T₁ in rotational transitions. *J Chem Phys* 1975;62:4380–7. <https://doi.org/10.1063/1.430338>.
- [20] Liuima FA, Bushkovitch AV, Rouse AG. Pressure Broadening of OCS in Foreign Gas Mixtures. *Phys Rev* 1954;96:434–5. <https://doi.org/10.1103/PhysRev.96.434>.
- [21] Burns MJ, Coy SL. Rotational relaxation rates for the OCS J=0–1 pure rotational transition broadened by argon and helium. *J Chem Phys* 1984;80:3544–51. <https://doi.org/10.1063/1.447199>.
- [22] Ross KA, Willey DR. Low temperature pressure broadening of OCS by He. *J Chem Phys* 2005;122:204308. <https://doi.org/10.1063/1.1901659>.
- [23] Casleton KH, Chien K-R, Foreman PB, Kukolich SG. Rotational relaxation measurements on OCS using a beam maser. *Chem Phys Lett* 1975;36:308–11. [https://doi.org/10.1016/0009-2614\(75\)80243-0](https://doi.org/10.1016/0009-2614(75)80243-0).
- [24] Story IC, Metchnik VI, Parsons RW. The measurement of the widths and pressure-induced shifts of microwave spectra lines. *J Phys B At Mol Phys* 1971;4:593–608. <https://doi.org/10.1088/0022-3700/4/4/023>.
- [25] Broquier M, Picard-Bersellini A, Whitaker BJ, Green S. Rotational inelastic cross sections for OCS–Ar, OCS–He, OCS–H₂ collisions: A comparison between theory and experiment. *J Chem Phys* 1986;84:2104–7. <https://doi.org/10.1063/1.450421>.
- [26] Liu W, Marcus RA. Theory of the relaxation matrix and its relation to microwave transient phenomena. II. Semiclassical calculations for systems of OCS and nonpolar collisions partners. *J Chem Phys* 1975;63:4564–4564. <https://doi.org/10.1063/1.431144>.
- [27] Green S. On the amount of information in rotational relaxation experiments with application to microwave transient T₁ and T₂ rates. *J Chem Phys* 1978;69:4076–82. <https://doi.org/10.1063/1.437140>.
- [28] Higgins K, Klemperer W. The intermolecular potential of He–OCS. *J Chem Phys* 1999;110:1383–8. <https://doi.org/10.1063/1.478013>.
- [29] Flower DR. The rotational excitation of OCS by He at low temperatures. *Mon Not R Astron Soc* 2001;328:147–9. <https://doi.org/10.1046/j.1365-8711.2001.04879.x>.
- [30] Wilzewski JS, Gordon IE, Kochanov RV, Hill C, Rothman LS. H₂, He, and CO₂ line-broadening coefficients, pressure shifts and temperature-dependence exponents for the HITRAN database. Part 1: SO₂, NH₃, HF, HCl, OCS and C₂H₂. *J Quant Spectrosc Radiat Transf* 2016;168:193–206. <https://doi.org/10.1016/j.jqsrt.2015.09.003>.

- [31] Allen L, Eberly JH. Optical Resonance and Two-Level Atoms. New York: Dover Publications, Inc.; 1987.
- [32] McGurk JC, Schmalz TG, Flygare WH. Fast passage in rotational spectroscopy: Theory and experiment. *J Chem Phys* 1974;60:4181–8. <https://doi.org/10.1063/1.1680886>.
- [33] Wolf F. Fast sweep experiments in microwave spectroscopy. *J Phys Appl Phys* 1994;27:1774–1780. <https://doi.org/10.1088/0022-3727/27/8/029>.
- [34] Park GB, Steeves AH, Kuyanov-Prozument K, Neill JL, Field RW. Design and evaluation of a pulsed-jet chirped-pulse millimeter-wave spectrometer for the 70–102 GHz region. *J Chem Phys* 2011;135:024202. <https://doi.org/10.1063/1.3597774>.
- [35] Grabow J-U. Fourier Transform Microwave Spectroscopy Measurement and Instrumentation. In: Quack M, Merkt F, editors. *Handb. High-Resolut. Spectrosc.*, John Wiley & Sons, Ltd; 2011. <https://doi.org/10.1002/9780470749593.hrs037>.
- [36] McGurk JC, Mäder H, Hofmann RT, Schmalz TG, Flygare WH. Transient emission, off-resonant transient absorption, and Fourier transform microwave spectroscopy. *J Chem Phys* 1974;61:3759–67. <https://doi.org/10.1063/1.1682562>.
- [37] Schwendeman RH. Transient Effects in Microwave Spectroscopy. *Annu Rev Phys Chem* 1978;29:537–58. <https://doi.org/10.1146/annurev.pc.29.100178.002541>.
- [38] Mäder H. Microwave fourier transform spectroscopy: Linewidth effects in the low pressure limit. *J Quant Spectrosc Radiat Transf* 1984;32:129–40. [https://doi.org/10.1016/0022-4073\(84\)90077-3](https://doi.org/10.1016/0022-4073(84)90077-3).
- [39] McGurk JC, Hofmann RT, Flygare WH. Transient absorption and emission and the measurement of T1 and T2 in the J O→1 rotational transition in OCS. *J Chem Phys* 1974;60:2922–8. <https://doi.org/10.1063/1.1681462>.
- [40] Hoke WE, Bauer DR, Ekkers J, Flygare WH. The measurement and interpretation of T1 and T2 in the inversion doublets of 15NH3 and the rotational transitions in OCS. *J Chem Phys* 1976;64:5276–82. <https://doi.org/10.1063/1.432156>.
- [41] Mäder H, Lalowski W, Schwarz R. Investigation of T1 and T2 Relaxation for Ethylene Oxide Rotational Transitions. *Z Für Naturforschung A* 1979;34:1181–1184. <https://doi.org/10.1515/zna-1979-1006>.
- [42] Mäder H, Bomsdorf H, Andresen U. The Measurement of Rotational Relaxation Time T2 for CH3C15N Self-and Foreign Gas Collisions. *Z Für Naturforschung A* 1979;34:850–857. <https://doi.org/10.1515/zna-1979-0709>.
- [43] Mehrotra SC, Bestmann G, Dreizler H, Mäder H. A Contribution to the Investigation of T2-Relaxation: Rotational Transitions of OCS and SO2. *Z Für Naturforschung A* 1984;39:633–636. <https://doi.org/10.1515/zna-1984-0707>.
- [44] Mehrotra SC, Dreizler H, Mäder H. Investigations of self-, H2- and He-broadening for rotational transitions of HCCC15N, CF3D and CF3CCH by the microwave transient emission technique. *J Quant Spectrosc Radiat Transf* 1985;34:229–31. [https://doi.org/10.1016/0022-4073\(85\)90003-2](https://doi.org/10.1016/0022-4073(85)90003-2).
- [45] Mehrotra SC, Dreizler H, Mäder H. J-Dependence of T2-Parameters for Rotational Transitions of SO2 and CH3OH in K-Band. *Z Für Naturforschung A* 1985;40:683–685. <https://doi.org/10.1515/zna-1985-0705>.
- [46] Mehrotra SC, Mäder H. Study of T1-and T2-Relaxation by Microwave Pulse Techniques: Rotational Transition J=0-1 of HCCF, J-Dependence of Rotational Transitions of SO2, and I-Type Doublet Transitions of HC15N Perturbed by Self, H2, D2, and He. *Z Für Naturforschung A* 1988;43:454–468. <https://doi.org/10.1515/zna-1988-0510>.
- [47] Haekel J, Mäder H. Determination of Spectral Parameters in Microwave Fouriertransform Spectroscopy by Analysis of Time-Domain Signals. *Z Für Naturforschung A* 1988;43:203–206. <https://doi.org/10.1515/zna-1988-0304>.

- [48] Coy SL. Speed dependence of microwave rotational relaxation rates. *J Chem Phys* 1980;73:5531–55. <https://doi.org/10.1063/1.440073>.
- [49] Haekel J, Mäder H. Speed-dependent T2-relaxation rates of microwave emission signals. *J Quant Spectrosc Radiat Transf* 1991;46:21–30. [https://doi.org/10.1016/0022-4073\(91\)90063-V](https://doi.org/10.1016/0022-4073(91)90063-V).
- [50] Rohart F, Mäder H, Nicolaisen H. Speed dependence of rotational relaxation induced by foreign gas collisions: Studies on CH₃F by millimeter wave coherent transients. *J Chem Phys* 1994;101:6475–86. <https://doi.org/10.1063/1.468342>.
- [51] He J, Zhang C. The accurate calculation of the Fourier transform of the pure Voigt function. *J Opt Pure Appl Opt* 2005;7:613–616. <https://doi.org/10.1088/1464-4258/7/10/014>.
- [52] Marquardt DW. An Algorithm for Least-Squares Estimation of Nonlinear Parameters. *J Soc Ind Appl Math* 1963;11:431–41. <https://doi.org/10.1137/0111030>.
- [53] Zaleski DP, Prozument K. Pseudo-equilibrium geometry of HNO determined by an E-Band CP-FTmmW spectrometer. *Chem Phys Lett* 2017;680:101–8. <https://doi.org/10.1016/j.cplett.2017.05.040>.
- [54] Arenas BE, Gruet S, Steber AL, Giuliano BM, Schnell M. Chirped-pulse Fourier transform millimeter-wave spectroscopy of ten vibrationally excited states of *i*-propyl cyanide: exploring the far-infrared region. *Phys Chem Chem Phys* 2017;19:1751–6. <https://doi.org/10.1039/C6CP06297K>.
- [55] Zaleski DP, Neill JL, Muckle MT, Seifert NA, Brandon Carroll P, Widicus Weaver SL, et al. A Ka-band chirped-pulse Fourier transform microwave spectrometer. *J Mol Spectrosc* 2012;280:68–76. <https://doi.org/10.1016/j.jms.2012.07.014>.
- [56] Steber AL, Harris BJ, Neill JL, Pate BH. An arbitrary waveform generator based chirped pulse Fourier transform spectrometer operating from 260 to 295GHz. *J Mol Spectrosc* 2012;280:3–10. <https://doi.org/10.1016/j.jms.2012.07.015>.
- [57] Neill JL, Harris BJ, Steber AL, Douglass KO, Plusquellic DF, Pate BH. Segmented chirped-pulse Fourier transform submillimeter spectroscopy for broadband gas analysis. *Opt Express* 2013;21:19743–9. <https://doi.org/10.1364/OE.21.019743>.
- [58] Hernandez-Castillo AO, Abeysekera C, Hays BM, Zwier TS. Broadband multi-resonant strong field coherence breaking as a tool for single isomer microwave spectroscopy. *J Chem Phys* 2016;145:114203. <https://doi.org/10.1063/1.4962505>.
- [59] Boissoles J, Thibault F, Doucen RL, Menoux V, Boulet C. Line mixing effects in the 00³–00⁰ band of CO₂ in helium. II. Theoretical analysis. *J Chem Phys* 1994;100:215–23. <https://doi.org/10.1063/1.466989>.
- [60] Rohart F, Ellendt A, Kaghat F, Mäder H. Self and Polar Foreign Gas Line Broadening and Frequency Shifting of CH₃F: Effect of the Speed Dependence Observed by Millimeter-Wave Coherent Transients. *J Mol Spectrosc* 1997;185:222–33. <https://doi.org/10.1006/jmsp.1997.7395>.
- [61] Köhler T, Mäder H. Measurement of speed dependent rotational relaxation rates using a microwave spectrometer with a circular waveguide. *Mol Phys* 1995;86:287–300. <https://doi.org/10.1080/00268979500102021>.
- [62] Wehres N, Heyne B, Lewen F, Hermanns M, Schmidt B, Endres C, et al. 100 GHz Room-Temperature Laboratory Emission Spectrometer. *Proc Int Astron Union* 2017;13:332–45. <https://doi.org/10.1017/S1743921317007803>.
- [63] Wehres N, Maßen J, Borisov K, Schmidt B, Lewen F, U. Graf U, et al. A laboratory heterodyne emission spectrometer at submillimeter wavelengths. *Phys Chem Chem Phys* 2018;20:5530–44. <https://doi.org/10.1039/C7CP06394F>.

Roles of the authors:

Author	Role
Brian M Hays	Design and construction and testing of E-band spectrometer. Experimental measurements and data analysis. Drafting and correction of article.
Théo Guillaume	Design and construction of flow cell. Construction and testing of E-band spectrometer. Participation in experimental measurements and data analysis. Correction of article.
Thomas S. Hearne	Design and construction of flow cell. Scientific discussions, contribution to and correction of article.
Ilsa R. Cooke	Testing of E-band spectrometer. Scientific discussions, contribution to data analysis and correction of article.
Divita Gupta	Testing of E-band spectrometer. Scientific discussions, correction of article.
Omar Abdelkader Khedaoui	Scientific discussions, correction of article.
Sébastien D. Le Picard	Scientific discussions, correction of article.
Ian R. Sims	Scientific direction of project, contribution to and correction of article.